CORA Cork Open Research Archive
Cartlann Taighde Oscailte Chorcaí

| | |
|---|---|
| Title | Energy-neutral ultra-wideband asset tracking tag for museums |
| Authors | Imfeld, Jonah;Mayer, Philipp;Soltani, Zahra;Kumar, Sanjeev;Buckley, John L.;O'Flynn, Brendan;Magno, Michele |
| Publication date | 2025-08-13 |
| Original Citation | Imfeld, J., Mayer, P., Soltani, Z., Kumar, S., Buckley, J.L., O'Flynn, B. and Magno, M. (2025) 'Energy-neutral ultra-wideband asset tracking tag for museums', 2025 IEEE Sensors Applications Symposium (SAS). Newcastle, United Kingdom, 08-10 July, pp. 1–6. https://doi.org/10.1109/SAS65169.2025.11105147 |
| Type of publication | Conference item |
| Link to publisher's version | https://ieeexplore.ieee.org/abstract/document/11105147 - 10.1109/SAS65169.2025.11105147 |
| Rights | © 2025, IEEE. Personal use of this material is permitted. Permission from IEEE must be obtained for all other uses, in any current or future media, including reprinting/republishing this material for advertising or promotional purposes, creating new collective works, for resale or redistribution to servers or lists, or reuse of any copyrighted component of this work in other works. |
| Download date | 2026-11-05 13:21:54 |
| Item downloaded from | https://hdl.handle.net/10468/18331 |

UCC
University College Cork, Ireland
Coláiste na hOllscoile Corcaigh

# Energy-Neutral Ultra-Wideband Asset Tracking Tag for Museums

Jonah Imfeld*, Philipp Mayer*, Zahra Soltani†, Sanjeev Kumar†,
John L. Buckley†, Brendan O'Flynn†, Michele Magno*
*Dept. of Information Technology and Electrical Engineering, ETH Zürich, Zürich, Switzerland
† Tyndall National Institute, University College Cork, Cork, Ireland

***Abstract*— Asset tracking is particularly important in museums, as it enhances security and simplifies the management of valuable artworks in both exhibition and storage. This paper details the development and evaluation of a custom-designed asset tracking tag that meets museum-specific requirements. To ensure energy-neutral operation, enabling minimal maintenance, the suggested implementation utilizes indoor light harvesting and event-based sampling. The presented tag operates at an ultra-low quiescent current of just 504 nA in motion-detection mode. For on-demand sampling, an energy-efficient wake-up receiver (WuR) enables remote activation at a total system current consumption as low as 2 µA. Localization samples were optimized to only consume 1.3 mJ per 2D-localization. The expected battery-life was assessed through simulations using a low-light indoor lighting dataset over the span of one year with a small 9.7 cm² photovoltaic (PV) cell. The results indicate that the tag achieves energy-neutral operation on a 20 mAh battery, supporting up to 60 localizations per day. With the WuR enabled, the tag is projected to operate for up to two years between charges, depending on the required localization frequency.**

***Index Terms*—Energy harvesting, ultra-wideband (UWB), Internet of Things (IoT), localization, asset tracking, ultra-low power, energy harvesting, energy-neutral, wake-up receiver, sensor systems and applications.**

## I. Introduction

Indoor localization has shown to be of particular interest in recent years due to its potential to facilitate tasks such as asset tracking or indoor navigation in public spaces [1]. Long time established satellite localization networks such as the global navigation satellite system (GNSS) are not suitable for indoor localization, because of the reduced performance caused by non-line of sight conditions indoors and the high power requirements. Many emerging technologies have been extensively researched in recent years to address this gap [2]. Until recently, most methods based on traditional baseband modulated communication system such as Wi-Fi or Bluetooth Low Energy (BLE) relied on the received signal strength (RSS) for distance estimation. While RSS-based localization is easy to implement for relative distance estimation, it provides limited accuracy [3], [4]. As a result of the need for precision location-aware Internet of Things (IoT) devices, newer generations of these technologies include improved ranging capabilities. Ranging using round-trip time (RTT) was added to wireless fidelity (Wi-Fi) in IEEE 802.11-2016 [5] as the fine-timing measurement (FTM) feature. For Bluetooth, angle of arrival (AoA) and angle of departure (AoD) features were introduced in the Bluetooth Core Specification v5.1 [6]. AoA and AoD allow localization through the use of triangulation. With Bluetooth Core Specification v6 [7], RTT and phase-based ranging (PRB) were officially introduced to enable more accurate distance measurements.

Ultra-wideband (UWB) has proven to be of particular interest for short distance, indoor ranging, as its underlying technology offers important advantages over Wi-Fi and BLE:

1) The use of wideband pulses instead of baseband modulation allows for more accurate RTT measurements, resulting in better spatial resolution [8].
2) The congested bands used by BLE and Wi-Fi cause problems for the time-critical RTT measurements [9]. Due to the low number of deployed devices using UWB technology and the difference in working principle compared to baseband modulated technologies, UWB promises better reliability [10].

The latest range of phones from Apple, Google, and Samsung include UWB integrated circuit (IC)s to enable features such as personal asset tracking or secure key-less car entry [11]. The AURORA project, funded by the European Commission [12], aims to develop a tracker system for valuable artworks in museums. Indoor asset tracking is of great interest for museums as it promises to enhance security of the art pieces while they are in the showroom and to ease asset management while in storage. The application of asset tracking in museums provides a special case, as the mobility of the tracked object is expected to be low compared to asset tracking of personal objects or in industrial logistics. Because the tag needs to be attached to the art piece directly, it should be small, inconspicuous and require little maintenance. To meet these requirements, energy harvesting is employed to enable the battery to be as small as possible. Specifically, solar energy harvesting was selected, as museums provide a predictable and consistent environment when it comes to lighting due to predefined opening hours and light settings.

This research work presents the development of a UWB-based asset tracking system. In particular, the contributions of this work are as follows:

*(i)* The hardware and software design of an asset tracking tag fitted to the requirements of a museum.
*(ii)* An evaluation of the tag's characteristics in terms of power consumption and ranging accuracy, demonstrating a stand-by power consumption of only 1.86 µW using an

event-based system-design enabled by a tag-centralized topology.

*(iii)* A simulation-driven evaluation of energy-neutral operation using indoor solar harvesting under artificial lighting, assuming a typical illuminance of 90 lx.

The rest of this paper is structured as follows: Section II discusses recent literature on localization technologies, asset tracking, and solar energy-harvesting. Section III provides the relevant background. Section IV introduces the implementation of the tracking tag and the anchor network. Section V presents the evaluation of the hardware in terms of power consumption, ranging accuracy, and analyzes energy-neutral operation based on a literature indoor lighting dataset. Finally, Section VI gives a brief overview of the findings.

## II. Related Work

Some of the examined localization technologies such as the acoustic approach presented in [13], or visual ones as in [14], [15] are easily disturbed by environmental noise which is a problem for applications in busy areas. Integrations using Wi-Fi were found to be more suitable for fingerprinting rather than the tracking of tiny IoT devices [2], [16]. While BLE was found to offer a lower peak power consumption compared to UWB [4], evaluations show that heavy oversampling and data processing are required for accurate localization based on BLE RSS [4], [17], which mitigates the power advantage. The inclusion of PRB enables better BLE-based ranging at accuracies below 0.5 m, but it still lags behind UWB RTT implementations with errors smaller than 10 cm [4], [18]. Based on this assessment, UWB was selected as the technology of choice for this implementation.

For the solar energy harvesting, the authors in [19]–[21] have shown that the power density of photovoltaic (PV) cells is heavily influenced not only by the illuminance, but also by the spectrum of the ambient light. In [22] Ferre´ et al. compared various PV technologies under different types of artificial lighting. These publications indicate that an evaluation of the selected PV cell under the targeted spectral conditions is crucial for accurate performance predictions of energy harvesting systems.

In [23] Mayer et al. implemented and thoroughly analyzed a UWB-based asset tracker with PV energy harvesting. It features a motion-detection mode at 1.2 µA static power consumption and localization samples require an energy of 10.82 mJ per sample. This systems energy-neutrality was analyzed over a time frame of over 700 days in simulation and a one-week-long lab experiment.

In comparison to previous works, the tag developed in this work meets the requirements for a deployment in museums. Specifically, a small footprint is targeted. The selected solar cell has an area of only 9.7 cm². Additionally, all evaluations were performed under the assumption of LED lighting. To achieve long-term operation under these conditions, an event-based hardware structure with fine-grained power control of individual components is used. This allows the system to achieve a very low quiescent current in motion-detection mode, which combined with the batteries self-discharge dictates achievable battery life in the defined setting.

## III. Background

The two main approaches to localization when using UWB are time-difference of arrival (TDoA) and two-way ranging (TWR). In the TDoA scheme, the location of the tag is calculated from the time difference of the reception of a frame sent by the tag to synchronized anchors. TDoA enables better scalability when it comes to tag density and localization frequency, and minimal energy consumption on the tag side as only one transmission is required. On the downside, it requires regular and highly precise synchronization of the time base between anchors due to clock drift. To solve the trilateration problem, at least one additional anchor is required compared to the TWR approach [24].

As mentioned in the introduction, the frequency of localizations is expected to be generally low in the discussed scenario. Thus, TWR, or more specifically single-sided two-way ranging (SS-TWR), will be used. In SS-TWR the RTT of a single message exchange between the tag and the anchor is used to calculate the distance. The delay $T_{\mathrm{Delay}}$ between the arrival of the initial message at the anchor and the response by the anchor is either fixed or included in the response. From $T_{\mathrm{Delay}}$ and the time between the transmission and reception at the tag $T_{\mathrm{Round}}$, the propagation delay can be calculated as $T_{\mathrm{Prop}} = (T_{\mathrm{Round}} - T_{\mathrm{Delay}})/2$. To enhance accuracy, $T_{\mathrm{Delay}}$ can be corrected by the clock offset between the tag and the anchor [25]. The clock offset is automatically calculated from the channel impulse response (CIR) by the used Qorvo DW3110 UWB transceiver [26].

## IV. System Architecture

For a fully functional UWB localization system, in principle two parts are required: First, the tag that is attached to the object that needs tracking. Secondly, the tag needs at least three or four anchor points within range to enable 2D or 3D-localization, respectively. These contact points are typically called anchors and enable the calculation of the tag's position using trilateration from their location and their distance to the tag. The calculation of the tags position is done on a processing server and not the tag itself.

This work primarily focuses on the implementation of the ultra-low power tag. It is important to note that functionality is tag-centralized, meaning that whether sampling is necessary is decided by the tag itself rather than the surrounding network. This is key to enabling the ultra-low power implementation.

### A. Tag Hardware

Figure 1 presents a high-level block diagram of the hardware architecture employed for the tag. It is divided into the localization and the always-on subsystems, enabling energy-efficient event-based operation. The following section outlines the key functionalities provided by the components in each subsystem.

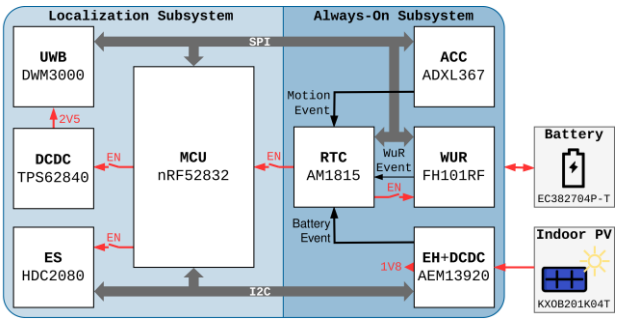



Fig. 1: Block diagram of the tag hardware.

**Always-On Subsystem** - In the sleep state, motion-based events can be generated by the ANALOG DEVICES ADXL367 accelerometer. It features motion detection functionality with an adjustable acceleration threshold, sampling frequency, and filtering with a claimed current consumption of 181 nA. The E-PEAS AEM13920 energy harvesting IC supplies the 1.8 V system voltage. It charges the battery from a solar cell using maximum power-point tracking (MPPT) if the lighting conditions are sufficient. In addition, it monitors the battery's charge state. The RFICIENT FH101RF wake-up receiver (WuR) is used to allow a wake-up of the system from a remote on-off keying (OOK) modulated source at a current consumption of only 2.6 µA while listening on the 868 MHz band. The bit rate of the OOK signal is configurable, presenting a trade-off between wake-up latency and power consumption. The most central part of the always-on subsystem is the AMBIQ AM1815 real-time clock (RTC). It monitors events from the accelerometer, the energy-harvesting IC, the WuR and allows for timed wake-ups. On an event, it toggles power to the microcontroller (MCU) for processing. Additionally, the RTC controls power to the WuR to allow fine-grained system power states with different functionality based on the harvested energy and defined requirements.

**Localization Subsystem** - The NORDIC SEMICONDUCTOR nRF52832 is a Cortex-M4 based MCU that processes the generated events and controls power to the QORVO DWM3000 UWB module and a TEXAS INSTRUMENTS HDC2080 temperature and humidity sensor. It is implemented as part of an INSIGHTSIP ISP4520 system-in-package (SiP) that also contains a SEMTECH SX1261 long range (LoRa) transceiver. If an insufficient number of anchors are available for localization, the LoRa communication IC can be used to indicate to the server that either the device has been moved out of range of the anchors or that there is a problem with the anchor network. Figure 2 shows the assembled tag PCB.

### B. Anchor Network

For the anchors, the QORVO DWM3001CDK development board was used. It combines a NORDIC SEMICONDUCTOR nRF52840 MCU with the QORVO DW3110 UWB transceiver and a printed circuit board (PCB) antenna. The anchors are assigned one of following two roles:

**Standard Anchor** - Once powered on, the standard anchor starts advertising its own position and device-specific address to nearby anchors on a fixed interval. It is configured to only respond to messages containing its address using the IEEE802.15.4-2020 medium access control (MAC) frame format with 2-byte addressing.

**Coordinator** - The coordinator listens and responds to a given address as well as broadcast messages if required. It incorporates an additional LoRa wide-area network (LoRaWAN) transceiver to communicate with a LoRaWAN gateway that connects the network to the data processing server. Based on the broadcast messages from the standard anchors, it builds information about the surrounding network.

### C. Tag Software Routine

Once power to the MCU is enabled, the source of the event that caused the wake-up, the battery voltage, temperature, humidity, and the distance to a pre-configured number of anchors with given oversampling are collected and sent to the coordinator via UWB where it is relayed to the cloud. Because the tag's MCU is not powered most of the time, it is assumed to have no information about the surrounding UWB network. Thus, the first SS-TWR sample is initiated on the broadcast address of the personal-area network (PAN). The coordinator replies to this message with the information required for the TWR exchange and the addresses of more nearby anchors. From there, the tag initiates the SS-TWR sessions with the anchors' addresses.

## V. EXPERIMENTAL RESULTS

### A. Ranging Accuracy

To verify point-to-point ranging accuracy, the implemented SS-TWR algorithm was used to calculate the distance between the Tag and a fixed anchor at distances of 1, 5, and 10 m apart. The ground truth distance was measured between the antennas of the two devices using a laser distance meter. Figure 3 shows the distribution of the samples at each distance. The worst-case distance error was found to be 25.8 cm, and the worst-case standard deviation is 6.6 cm.

### B. Static Power Consumption

To enable accurate modeling of the energy budget, the static power consumption of the circuit was measured in all possible hardware configurations. The measurement was performed

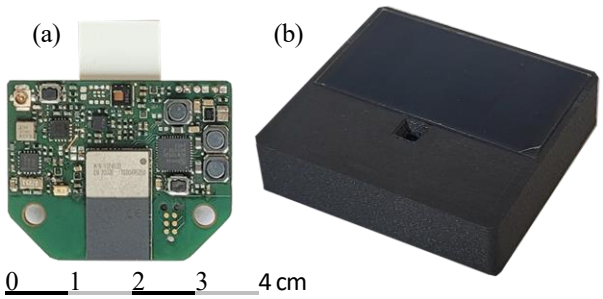



Fig. 2: (a) The populated tag PCB; (b) The PCB, battery and solar panel assembled in a case of size 45 × 41 × 11 mm.

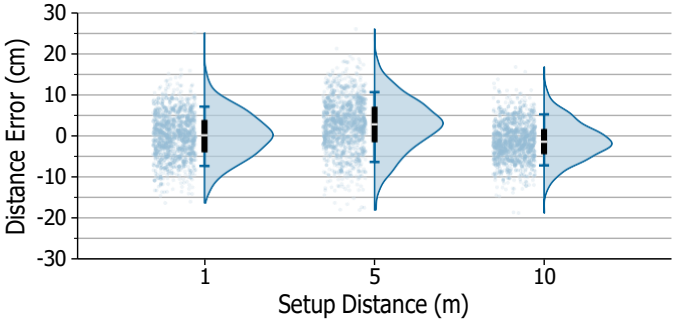



Fig. 3: Verification of the SS-TWR scheme in a point-to-point measurement without oversampling. The antenna delay was calibrated at a distance of 1 m beforehand.

with a KEYSIGHT N6781A source measurement unit (SMU) connected to the battery input. Measurements were taken at 3.2 V, 3.7 V, and 4.2 V. Table I lists the resulting power consumption. Each measurement was performed at a sampling rate of 12.5 kHz and averaged over three minutes.

### C. Dynamic Power Consumption

**Localization** - Figure 4 shows the typical power consumption profile during a localization sample. Clearly visible are the three pairs of spikes caused by the transmit and receive operations required for the SS-TWR in a 2D-localization setting. The last spike is caused by the transmission of the collected data from the tag to the coordinator. A typical sample has a duration of 34 ms and consumes 1.26 mJ of energy from the battery if no messages require retransmission. Each additional distance sample requires an additional energy of 185 µJ. As a result, the energy required for a localization with $m$ anchors and oversampling $p$ can be approximated as $E_{\text{Loc}} = 705\,\mu\text{J} + 185\,\mu\text{J} \cdot m \cdot p$.

**WuR Duty Cycling** - To minimize the sleep current consumption while still allowing for the remote wake up functionality enabled by the WuR, duty cycling can be used. The energy required to enable and configure the WuR on was measured at 1.07 mJ. Turning the IC off only requires reconfiguring the output of the RTC. This comes at a cost of 148 µJ. From these results, it can be calculated that duty cycling is only viable for long periods. For example, duty cycling with a period of one hour and an on-time of 25 % would reduce the power consumption by 2.4 µW.

Another option is to enable the WuR for one minute after a localization event. This offers the advantage of the processing

| System Configuration | | | | | $V_{\text{BAT}}$ | | |
|---|---|---|---|---|---|---|---|
| EH | RTC | ACC | WuR | MCU | 3.2 V | 3.7 V | 4.2 V |
| ✓ | ✓ | 1.5 Hz | ✗ | ✗ | 1.89 µW | 1.86 µW | 2.16 µW |
| ✓ | ✓ | 1.5 Hz | 256 b/s | ✗ | 7.14 µW | 7.37 µW | 7.5 µW |
| ✓ | ✓ | 1.5 Hz | 1 kb/s | ✗ | 9.77 µW | 9.89 µW | 10.2 µW |
| ✓ | ✓ | 1.5 Hz | ✗ | Idle | 454.5 µW | 456 µW | 459.1 µW |

TABLE I: Power consumed from the battery for given static system configurations at three battery voltage levels.

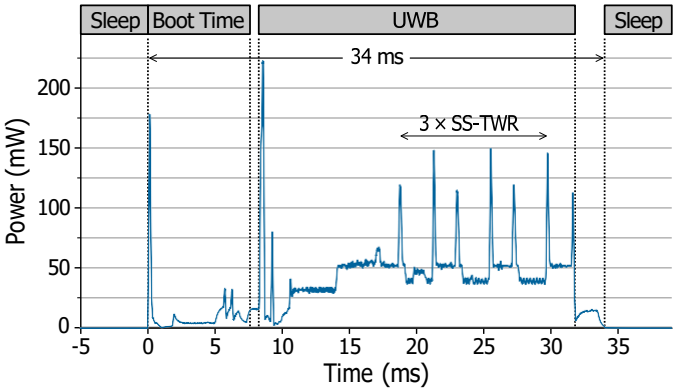



Fig. 4: Power consumption profile during a localization sample to three anchors without oversampling.

server being able to reach the tag after for configuration purposes. When this feature is enabled, the energy per sample is increased by 1.26 mJ, or a factor of 2.

### D. Energy Harvesting and Self-Sustainable Operation

To evaluate the self-sustainability of the proposed sensor node, each functional block was analyzed in terms of power consumption and efficiency. The resulting in-depth characterization was then used to develop a system model -following the model-based design approach presented in [27]- to validate the node's long-term energy neutrality and assess key design choices affecting overall performance. A summary of the specifications used for this assessment is provided in Table II.

**Solar Cell** - To optimally match the solar cell with the energy harvesting circuit, the KXOB201K04TF cell was first characterized under varying load and lighting conditions, as summarized in Figure 5. Targeting indoor operation in museums with limited exposure to natural light, the solar cell's performance was analyzed using both the broadband AM1.5 reference spectrum and a light source consisting of high color rendering index (CRI) LEDs designed for color-accurate illumination (NICHIA OPTISOLIS NF2W757GT-F1, 5000 K, CRI 98+). For the measurement, the cell was placed in a darkened chamber and artificially illuminated, while its output was monitored and loaded using a KEYSIGHT B2902A SMU. The inset in Figure 5 shows the solar cell's typical response to a varying load at a constant illuminance of 100 lx,

| | Description |
|---|---|
| EH dataset | [28], #13 - low light office space illuminance (day) 91 ± 69 lx, 1 year data |
| EH transducer | ANYSOLAR KXOB201K04TF 23 × 42 × 1.2 mm, 2 g |
| EH circuit | E-EPAS AEM13920 MPPT 70 %, overcharge protection 4.2 V |
| Energy storage element | NGK ENERCERA EC382704P, 20 mAh 38 × 27 × 0.45 mm, 0.73 g |

TABLE II: Key specifications of the designed energy-harvesting-powered sensing node.

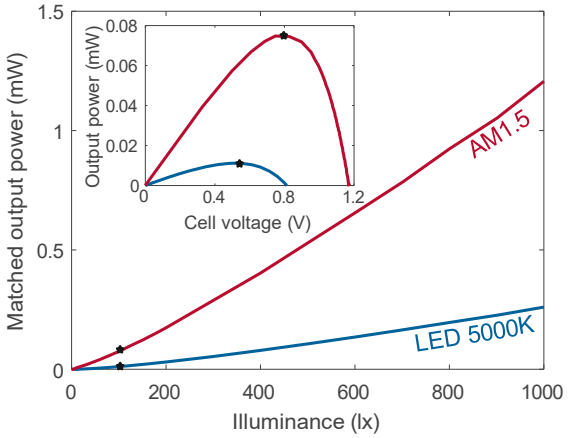



Fig. 5: Solar cell output power under matched conditions measured using the AM1.5 standard spectrum and a cold white LED spectrum, respectively. The inset shows the cell's response to a varying load at 100 lx.

revealing a maximum power point at 70 % of the open-circuit voltage. It is evident that the absence of the infrared spectral component in modern light sources significantly limits the silicon cell's output power, resulting in only a few tens of µW of output power in the targeted low-illuminance scenario. By combining the cell's spectrum-specific output power with a long-term indoor lighting dataset, the harvested power is assessed over extended periods. For further analysis, a subset of the dataset presented in [28] was used, comprising 365 days of data in a low-light office environment, with a typical daytime illuminance of 91±69 lx.

**Energy Harvesting Circuitry** - Following a similar approach, the AEM13920 IC was characterized across all relevant operational states by replacing the energy-harvesting transducer and battery with a KEYSIGHT B2902A SMU. To model the circuit's efficiency, a Random Forest regression model was trained to predict efficiency as a function of input voltage, input power, and battery voltage. The model was evaluated using 5-fold cross-validation, achieving an R-squared value of 0.94 using 10 % as test data.

**Energy Storage Element** - For further analysis, the energy storage element was modeled as a lithium-polymer battery following [27], based on the specifications of the NGK ENERCERA EC382704P cell, which has a capacity of 20 mA h and a self-discharge rate of 1 % of the SoC per month.
By combining circuit consumption in both static and dynamic operation with the modeled energy conversion and storage subsystem, the node's operation over one year was assessed, as summarized in Figure 6.

Figure 6 (a) shows a histogram of the daily energy collected by the energy-harvesting subsystem over the 365 days observation period. During the simulation, the circuit was configured in the motion-based wake-up mode. The results show that on 117 days, the system consumption exceeded the harvested energy. This typically occurred on weekends, when no artificial lighting was present in the room, and during winter. In contrast, on days with abundant environmental light, the battery could be charged with up to 800 mJ.

The battery SoC under varying localization event rates throughout the observation period is visualized in Figure 6 (b). When the deployment required more than 370 localization events per day, the system experienced power failures, necessitating manual battery recharging. However, if fewer than 60 localization events per day were triggered on average, energy-positive operation was achieved, resulting in a higher SoC at the end of the observation period than at the beginning. If the WuR was turned on for one minute after each localization, the operation would be energy-positive if fewer than 30 localization events were required per day. Scenarios with 60 to 370 localizations per day, as well as configurations where the WuR was set to always-on listening, could be sustained by the battery's stored energy over the one-year assessment period but were not energy-neutral.

## VI. CONCLUSION

In this paper, the hardware implementation of an asset tracking tag for valuable artwork artifacts in museums was presented and evaluated. The design was demonstrated to

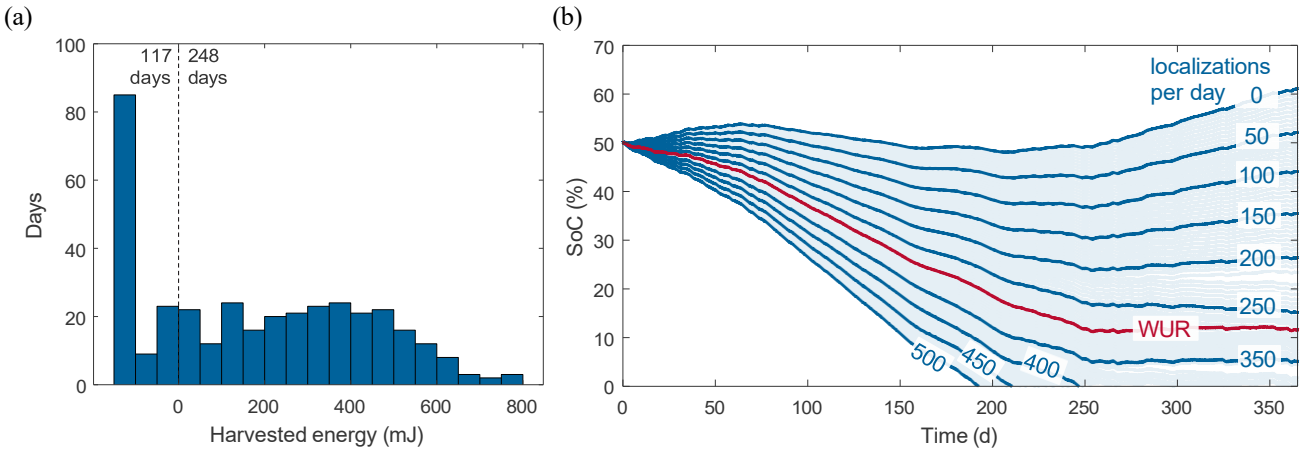



Fig. 6: Long-term system simulation: (a) Histogram of the daily energy balance; (b) Battery state of charge (SoC) over one year of operation for varying numbers of localization events per day.

feature a ranging error below 25 cm using SS-TWR without oversampling.

The event-oriented design enables the device to operate in sleep mode most of the time. If only motion detection and scheduled wake-ups are enabled, the current consumption was measured at only 504 nA. The integration of a novel wake-up receiver enables localization to be triggered on-demand from remote at a current consumption of 2 µA. The energy required for a sample was found to be 1.26 mJ.

A comparison of solar harvesting based on a silicon-based solar cell under indoor and outdoor lighting conditions has clearly shown that indoor lighting scenarios provide a difficult environment for energy harvesting. The extracted power is more than 7× lower at an illuminance of 100 lx. Still, simulation-based evaluation showed energy-neutral operation at up to 60 localization events per day in motion detection mode. If on-demand operation with low latency is required, the 20 mA h battery was shown to last more than two years between charges.

In future work, the tag's energy-neutral operation should be evaluated in a real deployment in a museum. Integration of the tag and anchor system with a central data processing server and the localization engine is in progress.

## ACKNOWLEDGMENTS

This work was carried out as part of the EU funded project AURORA (101094245). Aspects of this work have been financially supported by Taighde E´ireann – Research Ireland on behalf of the Government of Ireland under Grant 12/RC/2289-P2-INSIGHT, 13/RC/2077-2-CONNECT and 21/RC/10303-P2-VISTAMILK which are co-funded by the European Regional Development Fund (ERDF) under Ireland's European Structural and Investment Funds Program.

## REFERENCES

[1] S. G. Leitch *et al.*, "On indoor localization using wifi, ble, uwb, and imu technologies," *Sensors*, vol. 23, no. 20, 2023, doi: 10.3390/s23208598.

[2] P. S. Farahsari, A. Farahzadi, J. Rezazadeh, and A. Bagheri, "A survey on indoor positioning systems for iot-based applications," *IEEE Internet of Things Journal*, vol. 9, no. 10, pp. 7680–7699, 2022, doi: 10.1109/JIOT.2022.3149048.

[3] L. Flueratoru, V. Shubina, D. Niculescu, and E. S. Lohan, "On the high fluctuations of received signal strength measurements with ble signals for contact tracing and proximity detection," *IEEE Sensors Journal*, vol. 22, no. 6, pp. 5086–5100, 2022, doi: 10.1109/JSEN.2021.3095710.

[4] S. Cortesi, C. Vogt, and M. Magno, "Comparison between an rssi- and an mcpd-based ble indoor localization system," *Computers*, vol. 12, no. 3, 2023, doi: 10.3390/computers12030059.

[5] "Ieee standard for information technology—telecommunications and information exchange between systems local and metropolitan area networks—specific requirements - part 11: Wireless lan medium access control (mac) and physical layer (phy) specifications," *IEEE Std 802.11-2016 (Revision of IEEE Std 802.11-2012)*, pp. 1–3534, 2016, doi: 10.1109/IEEESTD.2016.7786995.

[6] "Bluetooth® Core Specification Version v5.1," 2019, accessed 25.02.2025. [Online]. Available: https://www.bluetooth.org/docman/handlers/downloaddoc.ashx?doc_id=457080.

[7] "Bluetooth® Core Specification Version v6," 2024, accessed 25.02.2025. [Online]. Available: https://www.bluetooth.org/DocMan/handlers/DownloadDoc.ashx?doc_id=588232.

[8] D. Dardari, R. D'Errico, C. Roblin, A. Sibille, and M. Z. Win, "Ultra-wide bandwidth rfid: The next generation?" *Proceedings of the IEEE*, vol. 98, no. 9, pp. 1570–1582, 2010, doi: 10.1109/JPROC.2010.2053015.

[9] W. Shao, H. Luo, F. Zhao, H. Tian, S. Yan, and A. Crivello, "Accurate indoor positioning using temporal–spatial constraints based on wi-fi fine time measurements," *IEEE Internet of Things Journal*, vol. 7, no. 11, pp. 11 006–11 019, 2020, doi: 10.1109/JIOT.2020.2992069.

[10] J. Tiemann, J. Friedrich, and C. Wietfeld, "Experimental evaluation of ieee 802.15.4z uwb ranging performance under interference," *Sensors*, vol. 22, no. 4, 2022, doi: 10.3390/s22041643.

[11] D. Barnwell, "What's the deal with ultra wideband," 2021, accessed 28.02.2025. [Online]. Available: https://www.bmw.com/en/innovation/bmw-digital-key-plus-ultra-wideband.html.

[12] "Aurora Project (101094245) Artwork Unique RecognitiOn and tRacking through chemicAl encoded data, miniaturized devices and blockchain alliance - AURORA," 2023, accessed 25.02.2025. [Online]. Available: https://cordis.europa.eu/project/id/101094245.

[13] G. Feferman, M. Blatt, and A. Eilam, "Indoor positioning with unsynchronized sound sources," in *2018 IEEE International Conference on the Science of Electrical Engineering in Israel (ICSEE)*, 2018, pp. 1–4, doi: 10.1109/ICSEE.2018.8646313.

[14] W. Zhang, G. Liu, and G. Tian, "A coarse to fine indoor visual localization method using environmental semantic information," *IEEE Access*, vol. 7, pp. 21 963–21 970, 2019, doi: 10.1109/ACCESS.2019.2899049.

[15] K. Majeed and S. Hranilovic, "Performance bounds on passive indoor positioning using visible light," *Journal of Lightwave Technology*, vol. 38, no. 8, pp. 2190–2200, 2020, doi: 10.1109/JLT.2020.2966365.

[16] M. Abbas, M. Elhamshary, H. Rizk, M. Torki, and M. Youssef, "Wideep: Wifi-based accurate and robust indoor localization system using deep learning," in *2019 IEEE International Conference on Pervasive Computing and Communications (PerCom*, 2019, pp. 1–10, doi: 10.1109/PERCOM.2019.8767421.

[17] F. Milano *et al.*, "Ble-based indoor localization: Analysis of some solutions for performance improvement," *Sensors*, vol. 24, no. 2, 2024, doi: 10.3390/s24020376.

[18] A. Santra, I. Kravets, N. Kotliar, and A. Pandey, "Enhancing bluetooth channel sounding performance in complex indoor environments," *IEEE Sensors Letters*, vol. 8, no. 10, pp. 1–4, 2024, doi: 10.1109/LSENS.2024.3456002.

[19] M. Masoudinejad, "Data-sets for indoor photovoltaic behavior in low lighting conditions," *Data*, vol. 5, no. 2, 2020, doi: 10.3390/data5020032.

[20] X. Ma, S. Bader, and B. Oelmann, "Power estimation for indoor light energy harvesting systems," *IEEE Transactions on Instrumentation and Measurement*, vol. 69, no. 10, pp. 7513–7521, 2020, doi: 10.1109/TIM.2020.2984145.

[21] B. Minnaert and P. Veelaert, "A proposal for typical artificial light sources for the characterization of indoor photovoltaic applications," *Energies*, vol. 7, no. 3, pp. 1500–1516, 2014, doi: 10.3390/en7031500.

[22] E. Ferre, M. Gasulla, and F. Reverter, "Comparative analysis of low-power pv cells of different technologies under different types of indoor artificial lighting," in *2024 IEEE International Instrumentation and Measurement Technology Conference (I2MTC)*, 2024, pp. 1–5, doi: 10.1109/I2MTC60896.2024.10561134.

[23] P. Mayer, M. Magno, and L. Benini, "Self-sustaining ultrawideband positioning system for event-driven indoor localization," *IEEE Internet of Things Journal*, vol. 11, no. 1, p. 1272–1284, Jan. 2024, doi: 10.1109/jiot.2023.3289568.

[24] J. Tiemann, F. Eckermann, and C. Wietfeld, "Atlas - an open-source tdoa-based ultra-wideband localization system," in *2016 International Conference on Indoor Positioning and Indoor Navigation (IPIN)*, 2016, pp. 1–6, doi: 10.1109/IPIN.2016.7743707.

[25] C. He and Z. Tang, "An uwb positioning algorithm based on clock compensation and filtering," in *2023 Cross Strait Radio Science and Wireless Technology Conference (CSRSWTC)*, 2023, pp. 1–3, doi: 10.1109/CSRSWTC60855.2023.10426834.

[26] D. Ltd, "Dw3000 family user manual," 2019, accessed 25.02.2025. [Online]. Available: https://www.qorvo.com/products/d/da008154.

[27] P. Mayer, M. Magno, and L. Benini, "Model-based design for self-sustainable sensor nodes," *Energy Conversion and Management*, vol. 272, p. 116335, 2022, doi: 10.1016/j.enconman.2022.116335.

[28] L. Sigrist, A. Gomez, and L. Thiele, "Dataset: Tracing indoor solar harvesting," in *Proceedings of the 2nd Workshop on Data Acquisition To Analysis*, ser. DATA'19, New York, NY, USA, 2019, p. 47–50, doi: 10.1145/3359427.3361910.